NMR Quantum Information Processing

Edwin Ng*
MIT Department of Physics
(Dated: May 14, 2012)

We demonstrate experimental techniques in quantum information processing on two qubits using liquid-state NMR spectroscopy of chloroform. We measure the J-coupling constant between the H and C nuclei and determine the coherence times T_1 and T_2^*. Using temporal averaging, we demonstrate the creation of pseudo-pure states and use these states to confirm the classical truth table of the two-qubit CNOT gate. We verify the correctness of the Deutsch algorithm and observe the output and oscillatory behavior of the Grover algorithm. Calibrations and a technique for quantifying signal quality based on measurement probabilities are discussed in detail.

I. INTRODUCTION AND THEORY

Quantum information is a generalization of the notion of classical information given the existence of resources such as quantum superposition. *Quantum computation* involves the design of algorithms that utilize these resources to solve problems faster than classically possible.

In the 1990s, liquid-state nuclear magnetic resonance (NMR) became a popular testbed for such designs, due to relatively long quantum coherence times and the maturity of the field.[1] In the 8.13 lab Pulsed NMR, we have already explored the fundamental concepts and techniques behind liquid-state NMR, including spin dynamics, pulsing, and the quantum coherence times T_1 and T_2^*. In this lab, we extend these techniques to a two-spin system with an eye towards studying quantum algorithms.

For two spins in a magnetic field $B_0\hat{\mathbf{z}}$, the Hamiltonian is the sum of the individual Hamiltonians plus a coupling:

$$H = \frac{\hbar J}{4}(\sigma_z \otimes \sigma_z) - \hbar\omega_1(\sigma_z \otimes I) - \hbar\omega_2(I \otimes \sigma_z), \quad (1)$$

where ω_1 and ω_2 are the Larmor frequencies of the first and second spins (H and C in our case), and J is the scalar coupling constant betweeen the two nuclei. If we let the system evolve freely for a time $\tau = \pi/J$, then the system undergoes the transformation

$$U_\tau = \exp\left(-i\frac{\pi}{4}\sigma_z \otimes \sigma_z\right). \quad (2)$$

In addition to this two-qubit gate, we also have access to our typical one-qubit rotation gates. In this lab, we will define 90° rotations about both $\hat{\mathbf{x}}$ and $\hat{\mathbf{y}}$, given respectively by

$$X = \exp\left(-i\frac{\pi}{4}\sigma_x\right) \quad ; \quad Y = \exp\left(-i\frac{\pi}{4}\sigma_y\right). \quad (3)$$

We use subscripts to specify the nucleus we are applying the gate to (e.g., X_1 for H) and a bar to denote the inverse, as in $\overline{X} = X^\dagger$.

* ngedwin@mit.edu

Liquid-state NMR generally features a mixed quantum state. Therefore, we make use of the density matrix formalism to describe our system. Let $\rho = \sum_j p_j|\psi_j\rangle\langle\psi_j|$ be the density matrix of a system composed of the states $|\psi_j\rangle$ with (classical) probabilities p_j. From quantum statistical mechanics,[2]

$$\rho = \frac{e^{-H/kT}}{\mathrm{tr}\, e^{-H/kT}} \simeq \frac{1}{4}\left(I + \frac{H}{kT}\right)$$

for two spins in the high temperature limit $kT \gg \hbar\omega_1$. (We can ignore the coupling energy, because $J \ll \omega_1$.) Since $\omega_1 \approx 4\omega_2$ from the gyromagnetic ratios of H and C, the thermal state of our NMR system is[3]

$$\rho \approx \frac{I}{4} + \frac{\hbar\omega_1}{16kT}\begin{bmatrix} 5 & 0 & 0 & 0 \\ 0 & 3 & 0 & 0 \\ 0 & 0 & -3 & 0 \\ 0 & 0 & 0 & -5 \end{bmatrix}. \quad (4)$$

If our density matrix is the diagonal matrix $\mathrm{diag}(a, b, c, d)$, then it can be shown that the induced signal after applying an X readout operator to the H or C nucleus is[3]

$$V_1(t) = V_0\left[(a-c)e^{i(\omega_1 - J/2)t} + (b-d)e^{i(\omega_1 + J/2)t}\right] \quad (5)$$

$$V_2(t) = V_0'\left[(a-b)e^{i(\omega_2 - J/2)t} + (c-d)e^{i(\omega_2 + J/2)t}\right] \quad (6)$$

where V_0 and V_0' are arbitrary amplification constants. Of course, due to T_2^*, the signals in Equations 5 and 6 are exponentially damped, leading to a *free induction decay* (FID), from which we can obtain information about ρ.

II. APPARATUS AND INTERFACE[3]

The apparatus we use is a Bruker Avance 200 NMR spectrometer with a sample of 7% by weight $^{13}CHCl_3$ dissolved in d6-acetone in a flame-sealed 5 mm glass tube. The sample is placed into a bore in a large superconducting magnet providing a static field $B_0\hat{\mathbf{z}}$ trimmed to be uniform to better than one part in 10^9 over one cm^3. The sample is spun rapidly to even out inhomgeneities, and additional coils are available to correct for higher order effects ("shimming").

In the transverse plane, we have two coils that allow us to apply RF pulses to each nucleus. After a pulse sequence is complete, these coils then switch to feeding the resulting FID to a sensitive pre-amplifier. Note that because a different amplifier is used for H and C, the relative signal strengths must be calibrated (see Section III.4), and, furthermore, a single pulse sequence must be run twice, taking the FID of H and C separately.

Our interface to the hardware is through MATLAB. To perform an experiment, we are allowed specification of several parameters:

1. *Phase References*: Two "output" phases specifying the global phase shifts to apply to all acquired FIDs, which defines the $\hat{\mathbf{x}}$ and $\hat{\mathbf{y}}$ axes of our system (see Section III.1).

2. 90° *Pulse Widths*: Two pulse times (on H and C) for 90° rotations, as obtained in Section III.2.

3. *Delay Times*: A list of delay times to wait after each pulse in the sequence, for applying U_τ, etc.

4. *Pulse Sequence*: Two lists (for H and C) of integer values specifying for each pulse how many multiples of the 90° pulse widths to apply.

5. *Phases*: Two lists (for H and C) specifying the "input" phase of each RF pulse, which defines rotation about the $\hat{\mathbf{x}}$, $\hat{\mathbf{y}}$, $-\hat{\mathbf{x}}$, or $-\hat{\mathbf{y}}$ directions.

We write pulse programs specifying each of these parameters. We also set the total delay time before each sequence to be 50 s, to allow for thermal relaxation.

After each pulse sequence is run, the MATLAB interface saves a spectrum file containing the Fourier-transformed FID spectrum sampled at 2048 points along a relative range of $[-250, 250]$ Hz about the center frequency of the acquired nucleus (about 200 MHz for H and 50 MHz for C). A single pulse sequence consists of two such files, one for H and one for C.

III. CALIBRATION AND MEASUREMENTS

III.1. Phase References

The first calibration we perform is to define the $\hat{\mathbf{x}}$ and $\hat{\mathbf{y}}$ axes of our system. We define a real FID spectrum (in phase with the reciever) to be the result of applying X to a spin initially along $\hat{\mathbf{z}}$, and an imaginary FID spectrum to be the result of applying Y.

This definition is represented by two global phases references ϕ_1 and ϕ_2, which is applied as a post-acquisition phase shift to all H and C FIDs, respectively. Since we do not yet have precise 90° pulse widths, we perform an X readout with a default pulse width of 5 µs and neutral phase references of 0° to obtain an H and C FID. To get a statistical measure of the uncertainty, we repeat the sequence ten times.

We apply a phase shift of $e^{i\phi}$ to each FID and then compute the total signal by integrating the left and right peaks over a range of 100 Hz about their centers using trapezoidal integration. We then compute the ratio R of the imaginary to the real parts of the integral and find the values of ϕ which minimizes R. Note that we also pick $\phi \in [180, 270]$ degrees to obtain $R > 0$. A plot of such a procedure is shown in Figure 1 below.

Repeating for all ten measurements, we take the average as our best determinations of the phase references, with uncertainty given by the standard deviation over $\sqrt{10}$. We find $\phi_1 = 229.8° \pm 0.2°$ and $\phi_2 = 233.7° \pm 0.3°$.

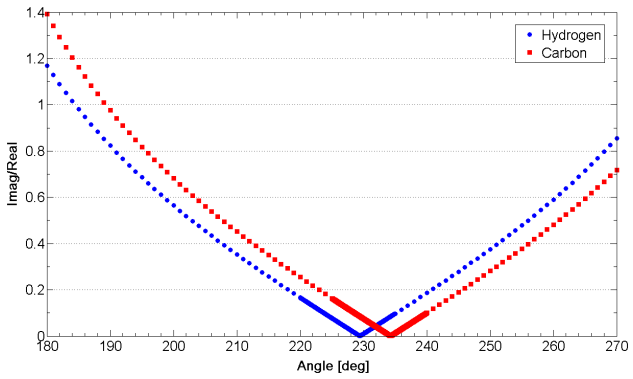

FIG. 1. R_1 and R_2 as a function of ϕ. Note that in the region around the minimum, we use a sampling resolution 0.01°. This measurement yields $\phi_1 = 229.45°$ and $\phi_2 = 234.29°$ with $R_1 = 2.76 \times 10^{-5}$ and $R_2 = 6.55 \times 10^{-5}$.

III.2. 90° Pulse Widths

After obtaining the correct phase references, we proceed to determine the 90° pulse widths for H and C. To do this, we apply a series of X readouts with varying lengths and find the pulse length that maximizes the FID signal. We pick the regions $[7, 10.5]$ µs and $[5.75, 10.5]$ µs for H and C, respectively, both with step sizes of 0.25 µs. We discard the first two points to ensure that all points are taken with the same 50 s relaxation time.

To determine the size of the FID signal, we integrate the left and right peaks using trapezoidal integration with integration range 10 Hz and centered at relative frequencies −108.0 Hz (left H), 106.9 (right H), −107.3 Hz (left C), and 107.6 Hz (right C). Errorbars in the summation are propagated from uniform errorbars on the FID, taken by sampling the standard deviation of the leftmost 500 points of the background.

We then fit a parabola $y = ax^2 + bx + c$ to each peak's variation with pulse width, with the 90° pulse width defined to be $-b/2a$. Theoretically, the left and right peaks should agree; experimentally, we find a small discrepancy. Thus, we average the two to obtain a final estimate of the 90° pulse width, with half their difference added to the statistical uncertainty. The fits for the left and right peaks of H are shown in Figure 2. We find the 90° pulse for H is (9.03 ± 0.05) µs; for C, we find (8.35 ± 0.11) µs.

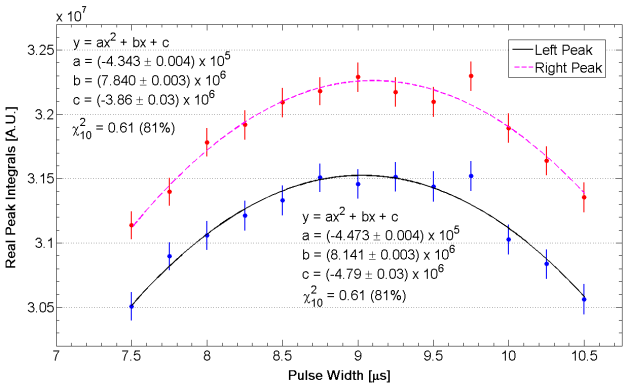

FIG. 2. Parabolic fits to left and right real peak integrals of H as a function of pulse widths.

III.3. T_1 Measurement

We measure the T_1 thermal relaxation time using the 180°–Δt–90° "inversion recovery" method. We invert the thermal population and wait a variable delay time, during which the spins will recover due to thermal relaxation; we then apply a 90° pulse to measure the recovered magnetization. The FID signal should therefore follow

$$y = A\left(1 - 2e^{-\Delta t/T_1}\right). \tag{7}$$

We pick Δt from 1 to 30 s, in steps of one. For the same reasons as in Section III.2, we discard the first point. We also obtain our peak integrals in the same way.

We fit the left and right peaks to Equation 7; again we find disagreement, so we average the results and add half their difference to the statistical uncertainty. We find $T_1 = (18.6 \pm 0.4)\,\mathrm{s}$ for H and $T_1 = (18.2 \pm 0.6)\,\mathrm{s}$ for C.

III.4. J, T_2^*, and Signal Calibration

Finally, we look at the thermal spectra for H and C, obtained from applying an X readout. This reference allows us to calibrate our signal strength to the physical density matrix as given by Equation 4.

From Equations 5 and 6, the ratio between the H and C peak integrals should be approximately 4. This is not observed experimentally because different amplifiers are used for the two nuclei. Thus, we want to renormalize all C FIDs by a factor N_C such that the thermal spectrum follows this physical ratio. We find that the left and right ratios are slightly different, at 10.4 and 9.9, so we first average the left and right peaks of each nucleus and then pick N_C to be the ratio of the H peak to the C peak divided by 4. Numerically, we find $N_C = 2.54 \pm 0.03$.

There is an additional normalization worth noting. This is the ratio between the arbitrary units in our FIDs to the physical unit $\hbar\omega_1/16kT$ in Equation 4. Since the H peak is expected to be 8 in the physical unit, we define the ratio K to be the averaged H peak in our arbitary units divided by 8. Numerically, $K = (7.75 \pm 0.03) \times 10^6$. This factor is used in interpreting the results of the computational stage of this lab (see Section IV).

We can also obtain the value of J and T_2^* from the thermal spectra. Since the FID is exponentially damped, we expect the spectral lines in the frequency domain are sharply peaked Lorentzians. The line width of the Lorentzian is then inversely related to the coherence time T_2^*, while the difference between the peak locations give J. We fit the spectra to a sum of Lorentzians of the form

$$y = \frac{\alpha\Gamma}{i(x - \omega_0) + \Gamma} \tag{8}$$

where α is a (possibly) complex number, Γ is a real line width, and ω_0 is the peak location. We therefore have $T_2^* = 1/\Gamma$ (or $1/2\pi\Gamma$, in Hz).

We show the fit for C in Figure 3 below. Note that we restrict the fit to only the area around the peak, to prevent the background from interfering. We choose the fit ranges $[-118, -104] \cup [98, 116]$ Hz for H and $[-112.4, -102.4] \cup [102.5, 112.5]$ Hz for C, with errorbars as described in Section III.2.

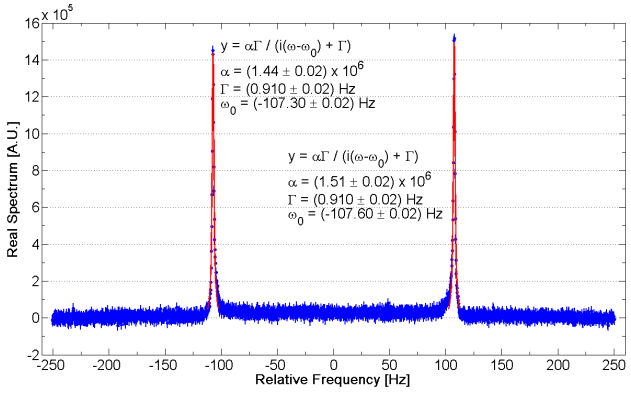

FIG. 3. Fit to the C thermal FID spectrum with the sum of two Lorentzians. Note that we use the same widths for both peaks but allow peak locations and amplitudes to vary; for this fit $\chi^2_{73} = 1.08$, with χ^2 probability 30%. Errorbars are drawn and visually make up much of the background "fuzz".

Using the values of Γ from the fits, we find $T_2^* = (0.180 \pm 0.003)\,\mathrm{s}$ for H and $T_2^* = (0.175 \pm 0.003)\,\mathrm{s}$ for C. Although substantially shorter than T_1, these values are still much larger than the time scale of computation, on the order of μs from 90° pulse widths.

Last, we can look also at the value of the J coupling constant. However, we find slightly different values from the H and C FID. Taking the average and adding half their difference to the statistical uncertainty, we find $J = (214.93 \pm 0.04)\,\mathrm{Hz}$.

The value of J is actually hardcoded into the MATLAB interface (for use in temporal averaging) as 214.9613 Hz, which is within our uncertainty. For consistency, therefore, we use the hardcoded value for our U_τ gates instead of the measured value.

IV. BASIS STATES AND CNOT

It is not obvious how quantum computation, which relies on manipulating pure states, can be carried out on a mixed thermal state like Equation 4. The answer is that this is not possible; instead, we rely on a technique called *temporal averaging* to produce *effective* "pseudo-pure" states. We note that if we begin with a diagonal density matrix $\rho = \mathrm{diag}(a, b, c, d)$, permute the diagonal elements ρ to $\mathrm{diag}(a, c, d, b)$ and $\mathrm{diag}(a, d, b, c)$ (via some unitary transforms), and then add all three matrices, we obtain a new matrix[2]

$$\overline{\rho} = (1 - a)I + (4a - 1)|00\rangle\langle 00|,$$

since $b + c + d = 1 - a$. This is not a physical density matrix; nevertheless, performing operations and readouts on $\overline{\rho}$ (i.e., performing operations and readouts on the three permuted matrices and adding together the FIDs) will give results exactly as if we were working with the pure state $|00\rangle\langle 00|$ (up to the normalization).

To complete the picture, we should take care of the normalization factor. Since $a = 1/4 + 5 \cdot \hbar\omega_1/kT$ from Equation 4, we need to multiply the results of temporal averaging by $N = 1/20K$ to obtain the normalized elements of the pseudo-pure density matrix. Numerically, $N = (6.45 \pm 0.03) \times 10^{-9}$.

For convenience, let us now use a, b, c, and d to refer to the diagonal terms of the pseudo-pure density matrix (the second term of $\overline{\rho}$, without the normalization), so that $a = 1$ and $b = c = d = 0$ represents the state $|00\rangle$, for example. This is exactly the peak integrals measured by Equations 5 and 6 after temporal averaging and renormalization by N_c and N.

IV.1. Computational Basis States

The first test of temporal averaging is the preparation and measurement of the computational basis states. We apply four different sequences: $I_1 I_2$, $X_1^2 I_2$, $I_1 X_2^2$ and $X_1^2 X_2^2$, which take the initial $|00\rangle$ state to the four basis elements. This is shown for H in Figure 4; comparing to Equation 5 verifies they are correct.

We can quantify the quality of these basis states by going one step further: we have access to all four peak integrals V_H^1, V_H^2, V_C^1, and V_C^2. Thus, we can set up the system of equations

$$V_H^1 = a - c \qquad V_H^2 = b - d$$
$$V_C^1 = a - b \qquad V_C^2 = c - d$$

and solve for a, b, c, and d. These are of interest because for a generic density matrix ρ, $\langle j|\rho|j\rangle$ tells us the *probability* of measuring the basis element $|j\rangle$. (We ignore the imaginary parts of the peak integrals, since they correspond to off-diagonal terms.) Since the system is rank-deficient, we eliminate one of the equations and add the normalization requirement $a+b+c+d = 1$. To estimate the systematic uncertainty, we eliminate each of the four equations in turn and average the solutions, adding the standard deviation to the statistical uncertainty. Table I shows these probabilities for the basis elements.

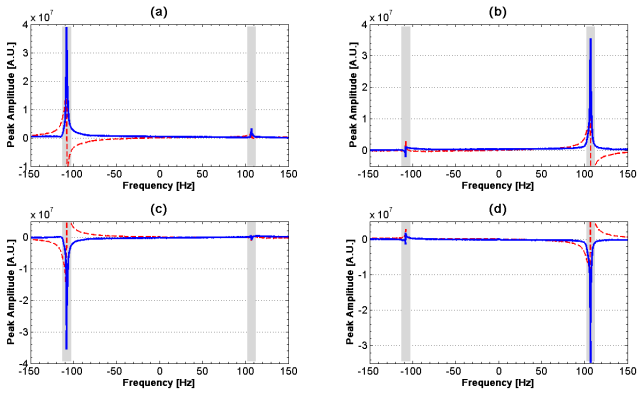

FIG. 4. H FID spectra of the four basis states after an X readout. The states are (a) $|00\rangle$, (b) $|01\rangle$, (c) $|10\rangle$, (d) $|11\rangle$. Real partis shown in solid blue; imaginary part is dashed red. The gray bars represent the integration region defined in Section III.2 and used throughout the following analysis.

	a	b	c	d
$\|00\rangle$	**0.62 ± 0.04**	0.18 ± 0.04	0.08 ± 0.04	0.11 ± 0.04
$\|01\rangle$	0.21 ± 0.04	**0.54 ± 0.04**	0.14 ± 0.04	0.11 ± 0.04
$\|10\rangle$	0.13 ± 0.05	0.13 ± 0.05	**0.58 ± 0.05**	0.17 ± 0.05
$\|11\rangle$	0.16 ± 0.05	0.14 ± 0.05	0.21 ± 0.05	**0.50 ± 0.05**

TABLE I. Populations for the basis elements.

IV.2. The CNOT Gate

The CNOT gate is used in many quantum algorithms and is defined on the computational basis by

$$C|i\rangle|j\rangle = |i\rangle|i \oplus j\rangle,$$

where $\oplus$ denotes addition modulo 2. That is, CNOT flips the second "target" qubit if and only if the first "control" qubit is 1. The CNOT gate with H control is implemented by the pulse sequence[4]

$$C = (Y_1 \overline{X}_1 \overline{Y}_1)(\overline{Y}_2 U_\tau Y_2) X_2. \qquad (9)$$

Applying this pulse sequence to each of the basis states yields the probabilities in Table II below, which confirm the classical truth table for CNOT.

	a	b	c	d
$C\|00\rangle$	**0.59 ± 0.03**	0.18 ± 0.03	0.10 ± 0.03	0.14 ± 0.03
$C\|01\rangle$	0.22 ± 0.03	**0.52 ± 0.03**	0.14 ± 0.03	0.12 ± 0.03
$C\|10\rangle$	0.16 ± 0.03	0.09 ± 0.03	0.25 ± 0.03	**0.50 ± 0.03**
$C\|11\rangle$	0.08 ± 0.03	0.16 ± 0.03	**0.51 ± 0.03**	0.25 ± 0.03

TABLE II. Populations for the CNOT gate.

V. THE DEUTSCH ALGORITHM

Suppose we are given a function $f : \{0,1\} \to \{0,1\}$. There are four possibilities:

$$f_0(0) = 0 \quad f_1(0) = 0 \quad f_2(0) = 1 \quad f_3(0) = 1$$
$$f_0(1) = 0 \quad f_1(1) = 1 \quad f_2(1) = 0 \quad f_3(1) = 1$$

We want to know whether f is *constant* (f_0 and f_3) or *balanced* (f_1 and f_2). Clearly, classical approach needs to evaluate both $f(0)$ and $f(1)$.

To solve the problem with a quantum algorithm, suppose we are given instead an *oracle* D representing f. A "query" is actually the application of one of the oracles:

$$D_0 = I_1 I_2 \quad D_1 = C \quad D_2 = CX_2 \quad D_3 = X_2$$

where C is the CNOT gate. If we can solve the problem with only one application of D, then we beat the classical case. The solution is given by the *Deutsch algorithm*, which consists of the pulse sequence

$$U(D_j) = \overline{Y}_1 Y_2 D_j Y_1 \overline{Y}_2. \tag{10}$$

Applying $U(D_j)$ on the state $|00\rangle$ gives $|f_j(0) \oplus f_j(1)\rangle|0\rangle$, so measuring the output gives $|00\rangle$ if f_j is constant and $|10\rangle$ if balanced, with only one query.

Table III below summarizes the outputs of the Deutsch algorithm on each oracle. Note that the dominant probability is indeed what we expect.

	a	b	c	d
D_0	**0.62 ± 0.04**	0.19 ± 0.04	0.08 ± 0.03	0.11 ± 0.03
D_1	0.09 ± 0.14	0.14 ± 0.04	**0.61 ± 0.04**	0.16 ± 0.04
D_2	0.11 ± 0.03	0.13 ± 0.03	**0.60 ± 0.03**	0.17 ± 0.03
D_3	**0.61 ± 0.03**	0.19 ± 0.03	0.09 ± 0.03	0.11 ± 0.03

TABLE III. Populations for the Deutsch algorithm.

VI. THE GROVER SEARCH ALGORITHM

Suppose we are given a set X of N items and a function $g : X \to \{0,1\}$, which marks one item x_0 with a 1 and the rest with 0. Given X and g, we want to *search* for x_0. Classically, this requires $O(N)$ queries to g.

In the quantum version, we let X to be our set of basis elements (so that $N = 4$ in our case) and replace g by the *Grover iterate*. The four grover iterates can be simplified (up to overall phases) into the pulse sequences[2]

$$G_0 = \overline{X}_1 \overline{X}_2 Y_1 Y_2 U_\tau \overline{X}_1 \overline{X}_2 Y_1 Y_2 U_\tau$$
$$G_1 = \overline{X}_1 \overline{X}_2 Y_1 Y_2 U_\tau X_1 \overline{X}_2 Y_1 Y_2 U_\tau$$
$$G_2 = \overline{X}_1 \overline{X}_2 Y_1 Y_2 U_\tau \overline{X}_1 X_2 Y_1 Y_2 U_\tau$$
$$G_3 = \overline{X}_1 \overline{X}_2 Y_1 Y_2 U_\tau X_1 X_2 Y_1 Y_2 U_\tau$$

The solution to the search problem is then given by the *Grover search algorithm*, with the pulse sequence

$$U(G_j, k) = G_j^k X_1^2 X_2^2 Y_1 Y_2, \tag{11}$$

where k is an integer specifying how many iterations of G_j to apply. It turns out that applying $k = O(\sqrt{N})$ gives the state corresponding to x_0 with high probability, and furthermore, the algorithm is periodic; this means that for some k_0, $k + 2k_0$, $k + 3k_0$, and so on also give x_0 with high probability. The results are shown in Figure 5.

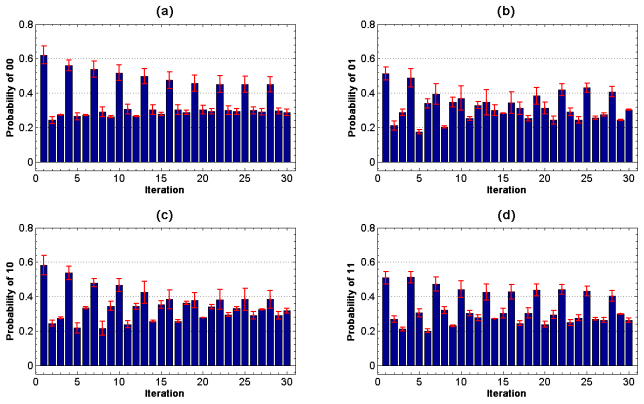

FIG. 5. Probabilities of correct answer as a function of k for Grover iterates (a) G_0, (b) G_1, (c) G_2, and (d) G_3.

VII. CONCLUSIONS

We characterize the NMR system by calibrating for phase references, 90° pulse, J, and signal strengths; we also measure the coherence times T_1 and T_2^* to be long enough for quantum information processing. We demonstrate the preparation of basis states by temporal averaging and the classical truth table of the CNOT gate. We verify the correctness of the Deutsch algorithm and the Grover search algorithm, and observe the later's oscillatory behavior. We also provide a method for quantifying contamination of the computation by looking at the populations of the density matrix.

[1] I.L. Chuang and M.A. Nielsen, *Quantum Computation and Quantum Information* (University Press, 2000).
[2] I.S. Oliveira, T.J. Bonagamba, et al., *NMR Quantum Information Processing* (Elsevier, 2007).
[3] M.I.T. Junior Lab Staff, "Quantum Information Processing with NMR," (2011).
[4] D.C. Marinescu and G.M. Marinescu, *Classical and Quantum Information* (Elsevier, 2012).